Method development in inverse modeling applied to supercritical fluid extraction of lipids

Abrahamsson, Victor; Andersson, Niklas; Nilsson, Bernt; Turner, Charlotta

Published in:
Journal of Supercritical Fluids

DOI:
10.1016/j.supflu.2016.01.006

2016

Document Version:
Peer reviewed version (aka post-print)

Abstract

Modeling of the supercritical fluid extraction of solid materials is an important aspect in order to understand and predict the process. A comparison of two empirical models, two semi-empirical models and two mechanistic models is performed using calibration of single experiments. It is concluded that the best fit is obtained using a simple empirical expression. Furthermore, single calibrations did not generate reliable parameters with physical meaning and a methodology is proposed for inverse modeling with complete calibration using several experiments. The experimental dataset contained 29 extractions of lipids from crushed linseeds with varying temperatures, pressures and flow rates. A general rate model and a proposed extension of the hot ball model were evaluated for this purpose. The methodology includes data acquisition, model structure estimation, model calibration and a cross-validation. In general, it was found that the solubility model of Sovová outperformed the other evaluated correlations, and for the general rate model the Toth partition isotherm was also found in the top model structures. However, no generalization could be made regarding the correlations describing the Nernst diffusion layer and diffusivity.

Abbreviations

BPR, back-pressure regulator; CV, cross-validation; DLT, diffusion-layer theory; DOE, design of experiments; EHBM, extended hot ball model; ELSD, evaporative light scattering detector; GA, genetic algorithm; GRM, general rate model; HBM, hot ball model; LHS, Latin hypercube sampling; ODE, ordinary differential equation; PSO, particle swarm optimization; RMSE, root mean square error; RMSEC, root mean square error of calibration; RMSECV, root mean square error of cross-validation; $scCO_2$, supercritical carbon dioxide; SFE, supercritical fluid extraction

1. Introduction

Supercritical fluid extraction (SFE) has been widely accepted as an alternative to conventional extraction techniques. The process is almost exclusively carried out using supercritical carbon dioxide ($scCO_2$) due to the fact that it is non-toxic, non-flammable, easy to handle, inexpensive and readily available and it has a low critical pressure and temperature. Additionally, the operator has the ability to alter solubility of various compounds by adjusting temperature, pressure or by adding co-solvent and thereby influencing the composition of the extract. The above-mentioned properties along with efficient mass transfer due to low viscosity and high diffusivities makes SFE a powerful extraction technique [1].

The applications of SFE span over a great field and has been extensively reviewed over the years [2-4], however much attention has been given to extraction from plant matrices [5]. It is worth emphasizing that the scales of SFE range from small scale within e.g. analytical chemistry in order to obtain compounds of interest for further analysis, to large scale in industrial applications for the removal of unwanted compounds or recovery of valuable compounds. The extraction is carried out batch-wise in either static, dynamic mode or a combination of both. In either case the material is contained in an extraction vessel with frits on either side to ensure that the material is kept in place [1].

Lund University, Department of Chemistry, Centre for analysis and synthesis, SE-221 00, Lund, Sweden.
Tel: +46 46-222 8125. Fax: +46 46-222 8209. E-mail: Victor.Abrahamsson@gmail.com
http://dx.doi.org/10.1016/j.supflu.2016.01.006

Naturally it is of great interest to fundamentally understand and to be able to describe the extraction process in order to optimize the method or to scale-up the process. Mathematical modeling of SFE provides an opportunity to address both issues and many examples exist in the literature trying to either explain or to predict observed phenomena of SFE applied to solid materials. Extensive reviews of mathematical models which have been proposed and in many cases also been applied, are found in the literature [5-8].

In general, the mathematical models used range from purely empirical to almost solely fundamental equations based on thermodynamics and mass transfer phenomena. Rather simply put, the rate of the SFE process is governed by solubility, mass transfer in the bulk fluid part of the packed bed, within particle mass transfer, mass transfer resistance in the interface between the intra and inter particulate space, partitioning of compounds between the fluid and the solid matrix and also possibly by adsorption to the solid matrix. Each of the before-mentioned phenomena and properties have been extensively studied in ideal systems and an abundance of correlations and models have been developed.

The numerous equations and expressions describing critical parts of the SFE process can be divided into model classes, where each class describes the phenomena mentioned above. The various model classes have been comprehensively reviewed. Modeling of diffusivity in supercritical fluids has been reviewed by e.g. Funazukuri et al. [9] and Medina [10]. Empirical models describing solubility in supercritical fluids have been reviewed by e.g. Škerget et al. [11]. Adsorption isotherms are widely used in many research fields and the most commonly used ones have been reviewed by e.g. Foo and Hameed [12]. Adsorption isotherms, usually linear, have only sparsely been considered in the modeling of SFE [13-18]. The expressions of adsorption isotherms may be used as partition isotherms [19], which may be more correct in cases where partition is occurring rather than adsorption.

The number of parameters that need to be determined or estimated increase with the complexity of the models. Unknown parameters such as diffusivity, solubility or the parameters of the partition isotherm can be determined by external experiments by independently studying e.g. the solubility in an ideal system. Another approach is to apply inverse modeling, also known as the inverse method, by studying e.g. extraction yield over time and then estimating the unknown parameters so that the simulated extraction curve matches the experimental equivalent. This is also known as model calibration of the model structure, which contains a set of equations, in order to estimate the unknown parameters and thereby gaining a well-defined process model [20]. A common trend in the literature is that the calibration is usually performed by minimizing a fitness function of residuals using a gradient based numerical solver, however, limiting the number of unknown parameters to between one and three.

The parameters are usually estimated by calibrating a model structure to each individual experiment, thus generating a unique set of parameters and a unique process model for each extraction curve. A few exceptions are available in the literature, for example one study kept a constant density and temperature but altered the flow rate between experiments and estimated the coefficients correlating the dimensionless numbers of Sherwood, Reynold and Schmidt [21].

The inverse method is commonly used in various areas of engineering to indirectly study underlying phenomena, for example in mechanistic modeling of chromatography to partially or fully determine parameters with comparably good success [22]. However, for the purpose of estimating parameters of SFE model structures it has been argued that an individual extraction curve contains relatively little information on its own to calibrate multiple

parameters through the inverse method with a good confidence. Depending on the model structure used it can be difficult to discriminate between various effects, e.g. between internal mass transfer and solubility [14].

Perhaps the most important and difficult issue is how to choose a model structure consisting of several model classes and thus forming many candidate model structures. In many cases the researcher has an idea of which phenomena might be crucial, motivated by chemical and engineering knowledge and experience. The situation becomes slightly more peculiar in more complex mass balance models where plenty of relationships and models describing the various phenomena are suggested in the literature. As an example of this abundance, there are over 20 reported relationships which in an empirical fashion describes the solubility of solids in $scCO_2$ [11].

In general, the model structure in various studies is arbitrarily chosen. Consequently, a poorly chosen expression describing e.g. the Nernst diffusion layer might result in erroneously estimated parameters for an expression describing internal diffusion through the inverse method.

There are relatively few studies comparing model structures used to describe the SFE process present in the literature. To mention a few, one previous study compared a mechanistic and a semi-empirical equation and also compared the results generated by simulations using the FEM and the MATLAB softwares [23]. Another study compared a mass balance model, the hot ball model and the Sovová's model [24].

In this work several models are compared including empirical one-term exponential functions, the semi-empirical hot ball model (HBM) and the diffusion-layer theory (DLT) model, and mechanistic models based on a packed bed with porous material. These were compared in regards to goodness of fit with experimental data. It is important to outline that many other models exist, of which many are frequently used but are not addressed in this work. Examples of such models are the shrinking core model [25] and the broken & intact model [26, 27]. Furthermore, the feasibility of complete calibration models instead of calibration performed using single experiments was evaluated.

The main aim of this paper is to address several issues that are essential to fundamentally understand and to predict the SFE processes applied to solid materials. Proposed is a general methodology including acquisition of experimental data using an already published and validated method [28], model structure selection, estimation of parameters by calibrating the model structure to a full set of experiments and a cross validation (CV).

2. Materials and methods

2.1. Chemicals and sample material

Ethanol (99.7%, Solveco, Rosenberg, Sweden) was used as a make-up flow in the SFE. Ultrapure CO_2 was provided by Air Products (Amsterdam, Netherlands). Crushed linseeds were bought in the local grocery store and used as they were. The glass beads used to fill up the remaining volume of the extraction vessel were from Marienfeld (Lauda-Königshofen, Germany).

The size of the crushed linseeds was measured firstly by sieving and also by an Olympus Infinity microscope with an Olympus SDF 0.5 PLA PO objective using the Infinity Analyze software (Olympus Corp., Japan). The density of the crushed linseeds was measured gravimetrically and volumetrically by placing the linseeds in a volumetric cylinder of ethanol and quickly measuring both the weight and volume of the added linseeds.

2.2. Instrumental setup

The instrumental setup with on-line detection and the extraction method used has previously been validated for the extraction of lipids from crushed linseed, described by Abrahamsson et al. [28]. The system consisted of two ISCO 260D syringe-pumps (Teledyne Isco, Thousand Oaks, CA) used for pumping liquid CO_2, a Waters 515 HPLC-pump (Milford, MA) used for pumping ethanol, a HP 5890 gas-chromatography oven (Hewlett-Packard, Wilmington, DE) functioning as oven, a Tescom 26-1700 series back pressure regulator (BPR) (Tescom Europe, Selmsdorf, Germany) and an Eltherm ELTC/3 thermoregulator (Eltherm Elektrowärmetechnik GmbH, Burbach, Germany) was used for heating the lining between the BPR and the evaporative light scattering detector (ELSD) of model Sedex 55 (Sedere, Alfortville, France). The post-depressurization heating was set to 363 K in order to avoid freezing, the nitrogen feed to the ELSD was 0.3 MPa, the drift tube temperature of the ELSD was 368 K and the gain factor was 5. A Rheodyne injection valve with a 0.65 mL loop was implemented into the system before the BPR. The liquid CO_2 pump was cooled by a Julabo F12 cooling system (Julabo, Vista, CA).

Approximately 0.6 g of weighted linseeds were placed in a 10 mm x 30 mm extraction vessel from Applied Porous Technologies (Onsala, Sweden). The void volume at the end of the extraction vessel was filled up with 3 mm Ø glass beads. This resulted in a packed bed of linseeds with the length of 25 mm.

The extraction conditions were based on a symmetrical full factorial design of experiments (DOE) with three factors and three levels. The factors were pressure (P) ranging from 15 to 30 MPa, temperature (T) from 313 to 353 K and compressed CO_2 pump volumetric flow rate (Q) from 0.5 to 1.5 mL/min, with three replicates at the center point (P = 22,5 MPa, T = 333 K, Q = 1 mL/min) thus resulting in a total of 29 extractions.

2.3. Kinetic models

Several models of varying complexity were employed in this study in order to compare performance. The models and the modeling approaches can be categorized into single calibration models and complete calibration models. Single calibration models refer to models or inverse modeling where one set of parameters are estimated per experiment, while complete calibration models refer to inverse modeling where the model and its parameters is calibrated and estimated using the complete set consisting of all the experiments.

2.3.1. Single calibration models

Several models were evaluated using individual experiments for calibration (**Table 1**). The simplest models were based on a one-term expression with one (Eq. 1) [29], or two (Eq. 2) [30] estimated parameters. The HBM (Eq. 3) [31] and the DLT (Eqs. 4-5) [32] which both considers the diffusivity inside a particle, were also estimated as single calibration models. Mathematical modeling using mass balance equations were evaluated in two configurations. The first configuration describes the simplest form of a packed bed reactor (Eqs. 6-13) whilst the modification (Eqs. 14-15) also takes into consideration the distribution constant, K_D, also known as the partitioning ratio, both as defined by the IUPAC gold book [33].

Table 1. A summary of single calibration models including simple empirical equations, semi-empirical and mass balance models.

Empirical equations			
one-term exponential [29]	$\frac{m}{m_0} = (1 - e^{-kt})$		(1)
one-term expression with two parameters [30]	$\frac{m}{m_0} = H(1 - e^{-kt})$		(2)
Semi-empirical equations			
Hot ball model [31]	$\frac{m}{m_0} = \frac{6}{\pi^2}\sum_{n}^{\infty}\frac{1}{n^2}e^{-n^2\pi^2 D_e t / R_p^2}$		(3)
Diffusion layer theory [32]	$\frac{m}{m_0} = 1 - \frac{\beta_{DLT} Q}{\beta_{DLT} V - Q}\left(\frac{V}{Q}e^{-(Q/V)t} - \frac{1}{\beta_{DLT}}e^{-\beta_{DLT} t}\right)$		(4)
	$\beta_{DLT} = \frac{AD_{12}}{h}$		(5)
Mass balance models			
Mass balance model of a packed bed			
Differential mass transfer in the bulk phase	$\frac{\partial c_b}{\partial t} = -u_{lin}\frac{\partial c_b}{\partial z} - \frac{3k_f(1-\varepsilon_c)}{R_p \varepsilon_c}(c_b - c_s)$		(6)
Initial conditions	$c_b = 0$	(at $t = 0$, for all z)	(7)
Boundary conditions	$c_b = 0$	(at $z = 0$)	(8)
	$\frac{\partial c_b}{\partial z} = 0$	(at z = L)	(9)
Differential mass transfer in the particle	$\frac{\partial c_p}{\partial t} = D_e\left(\frac{\partial^2 c_p}{\partial r_p^2} + \frac{2}{r_p}\frac{\partial c_p}{\partial r_p}\right)$		(10a)
Initial conditions	$c_p = c_{init}$	(at $t = 0$, for all r_p)	(11)
Boundary conditions	$\frac{\partial c_p}{\partial r_p} = 0$	(at $r_p = 0$)	(12)
	$\frac{\partial c_p}{\partial r_p} = \frac{k_f}{D_e}(c_b - c_s)$	(at $r_p = R_p$)	(13a)
Modifications of the mass balance model to include the distribution constant			
Differential mass transfer in the bulk phase	$\frac{\partial c_b}{\partial t} = -u_{lin}\frac{\partial c_b}{\partial z} - \frac{3k_f(1-\varepsilon_c)}{R_p \varepsilon_c}\left(c_b - \frac{c_s}{K_D}\right)$		(14)
Boundary conditions	$\frac{\partial c_p}{\partial r_p} = \frac{k_f}{D_e}\left(c_b - \frac{c_s}{K_D}\right)$	(at $r_p = R_p$)	(15)

In both cases the axial dispersion term is omitted and the particle porosity is not considered as the phase inside the particle is considered as homogenous. The density is only considered to determine the linear flow rate in the mass balance models.

Properties such as temperature and viscosity are not taken into account. The following assumptions are made for the single calibration mass balance models and the complete calibration models (see section 2.3.2):

- Isobaric and isothermal throughout the whole packed bed
- The solute is initially equally distributed within the sample matrix
- The physical properties such as for example density and viscosity of the fluid are constant throughout the extraction and length of the column
- Radial dispersion is neglected due to symmetry
- Axial dispersion is neglected due to low dwell time
- Channeling effects are evenly distributed along the column

2.3.2. Complete calibration models

In order to construct a model which could describe the SFE process over the whole design space of various extraction conditions, a complete calibration of model structures by using all of the experiments from the DOE was performed. These model structures contained equations from model classes describing solubility, partitioning, diffusivity and external mass transfer (**Fig. 1**). Two models were used in this study and they are presented below and referred to as the general rate model (GRM) and the extended hot ball model (EHBM) (**Table 2**).

The EHBM, much like the original HBM [31], considers a domain where the solute is homogenously distributed throughout the space. The proposed EHBM does not consider a saturation of the $scCO_2$ in the particle domain but rather considers the media of which mass transfer is occurring as gas expanded lipids [34]. Hence, the diffusivity inside the particle is not equal to that outside of the particle. However, the solubility of lipids in $scCO_2$ is still limited at the interface between the solid particle and the bulk fluid.

The GRM is frequently used in liquid chromatography [35, 36], and describes the mass transfer in the packed bed (Eqs. 6-9), the mass transfer inside the pores of the particle (Eqs. 10b, 12, 13b, 16-17) and also includes a solute-solid interaction inside the particle. As opposed to the EHBM the solubility and the partitioning of the solute is rather taken into consideration inside the particle. Therefore, two domains are acquired, one corresponding to the volume inside the pores of particle and one representing the solid matrix of particle. The partitioning of the solute between the fluid in the pores and the solid matrix is assumed to be in pseudo-equilibrium, which is described further down. In the GRM the solute dissolved in the $scCO_2$ inside the particle is confined to the pores. The effective diffusivity is then given by Eq. (20).

$$D_e = \varepsilon_p D_{12} \tag{20}$$

Table 2. A summary of the domain equations, initial and boundary conditions of the GRM and the EHBM.

General rate model			
Differential mass transfer in the bulk phase			
Domain equation	$\frac{\partial c_b}{\partial t} = -u_{lin}\frac{\partial c_b}{\partial z} - \frac{3k_f(1-\varepsilon_c)}{R_p\varepsilon_c}(c_b - c_s)$		(6)
Initial conditions	$c_b = 0$	(at $t = 0$, for all z)	(7)
Boundary conditions	$c_b = 0$	(at $z = 0$)	(8)
	$\frac{\partial c_b}{\partial z} = 0$	(at z = L)	(9)
Differential mass transfer in the particle			
Domain equation	$\frac{\partial c_p}{\partial t} = D_e\left(\frac{\partial^2 c_p}{\partial r_p^2} + \frac{2}{r_p}\frac{\partial c_p}{\partial r_p}\right) + \frac{1-\varepsilon_p}{\varepsilon_p}\frac{dq}{dt}$		(10b)
Initial conditions	$c_p = 0$	(at $t = 0$, for all r_p)	(16)
	$q = c_{init}$	(at $t = 0$, for all r_p)	(17)
Boundary conditions	$\frac{\partial c_p}{\partial r_p} = 0$	(at $r_p = 0$)	(12)
	$\frac{\partial c_p}{\partial r_p} = \frac{k_f}{\varepsilon_p D_e}(c_b - c_s)$	(at $r_p = R_p$)	(13b)
Extended hot ball model			
Differential mass transfer in the bulk phase			
Domain equation	$\frac{\partial c_b}{\partial t} = -u_{lin}\frac{\partial c_b}{\partial z} - \frac{3k_f(1-\varepsilon_c)}{R_p\varepsilon_c}\left(1 - \left(\frac{c_b}{c_{sat}}\right)^2\right)(c_b - c_s)$		(18)
Initial conditions	$c_b = 0$	(at $t = 0$, for all z)	(7)
Boundary conditions	$c_b = 0$	(at $z = 0$)	(8)
	$\frac{\partial c_b}{\partial z} = 0$	(at z = L)	(9)
Differential mass transfer in the particle			
Domain equation	$\frac{\partial c_p}{\partial t} = D_e\left(\frac{\partial^2 c_p}{\partial r_p^2} + \frac{2}{r_p}\frac{\partial c_p}{\partial r_p}\right)$		(10a)
Initial conditions	$c_p = c_{init}$	(at $t = 0$, for all r_p)	(11)
Boundary conditions	$\frac{\partial c_p}{\partial r_p} = 0$	(at $r_p = 0$)	(12)
	$\frac{\partial c_p}{\partial r_p} = \frac{k_f}{D_e}\left(1 - \left(\frac{c_b}{c_{sat}}\right)^2\right)(c_b - c_s)$	(at $r_p = R_p$)	(19)

The initial conditions for the EBHM and the GRM assumed that no initial solute is present in the bulk fluid prior to extraction (Eq. 7), while the EBHM assumes that c_p has an initial solute concentration (Eq. 11) whilst GRM does not since the solute is initially located in the solid matrix which is a different domain (Eqs. 16-17). The initial solute concentration is based on the linseed density and the extractable amount which has previously been determined [28].

The same assumptions for the complete calibration models were made as for the single calibration mass balance models (see section 2.3.1). The density and the viscosity of the $scCO_2$ for each temperature and pressure were obtained through the NIST WebBook of thermophysical properties of fluid systems [37].

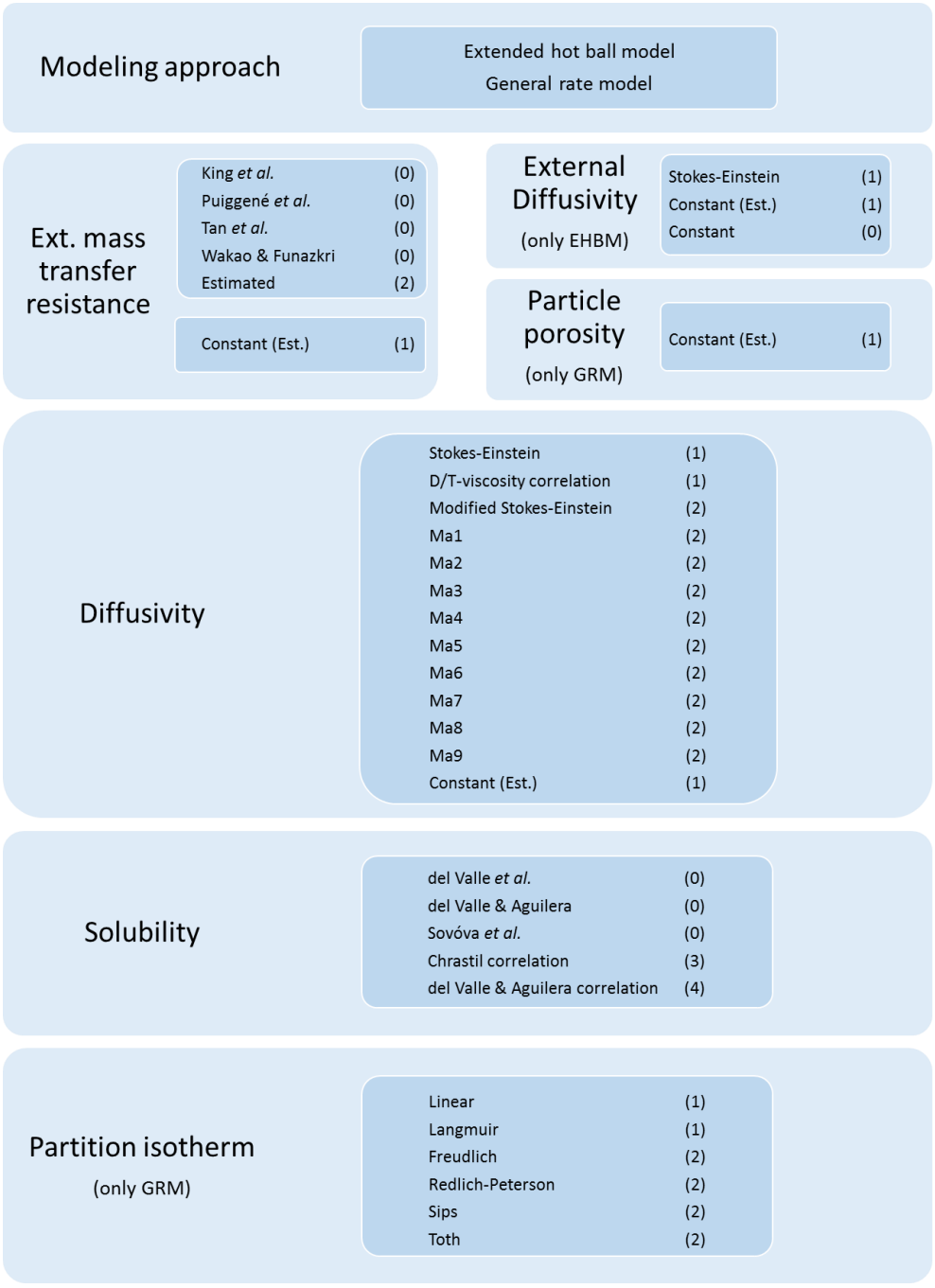

Fig. 1. Overview of the modeling approaches and the model classes used in the inverse modeling of the SFE process using complete calibration. The number of parameters estimated in each expression is stated within the parenthesis.

The Nernst diffusion layer, denoted k_f and also referred to as the film coefficient is the external mass transfer resistance due to a stagnant layer around the particle through which the solute needs to diffuse. Several models have been proposed in the literature, and in this work, the correlations of King et al. (Eq. 21) [38], Puiggené et al. (Eq. 22) [39], Tan et al. (Eq. 23) [40] and Wakao and Funazkri (Eq. 24) [41] have been evaluated with the addition of an approach

where two of the parameters (Eq. 25) otherwise reported in the literature were estimated by the inverse method (**Table 3**). The equations used in order to estimate k_f from these correlations are described in Appendix.

The diffusivity can be estimated through various expressions with varying dependent variables such as temperature, density and viscosity. Several models were evaluated (**Table 4**) based on either combined parameters of the Stokes-Einstein (SE) equation (Eq. 26), a modification of the SE (mSE) equation (Eq. 27) [42], the *D/T*-viscosity correlation (Eq. 28) [43], and nine different simple correlations (Eqs. 29-37) proposed by Magalhães et al. [44] here denoted Ma1-9. Corrections and other versions of the SE equation (Eq. A.4) are frequently used to describe the diffusivity in supercritical fluids, e.g. the expression of Wilke-Chang [45]. Vaz et al. proposed modifications of the Wilke-Chang (Eq. A.5) [42]. In this work the correlations of Wilke-Chang and the modification of the expression were simplified by lumping all constants into one or two parameters which were estimated during calibration. By performing these simplifications, the expression once again resembles the SE equation and its modification was therefore referred to as the SE equation and mSE equation, respectively.

As described before, in the GRM the effective diffusivity was estimated using Eq. (20) or by assuming that the binary and effective diffusivity were the same. While in the EHBM the binary diffusivity inside the particle and outside the particle are assumed to be different and thus estimated independently by the inverse method. However, in this case to maintain a sound amount of parameters the diffusivity was either assumed to be 10^{-6} m^2/s as was also assumed by Reverchon et al. [46], as an estimated constant independent from extraction conditions or estimated using the calibrated Stokes-Einstein equation (Eq. 26).

The solubility of the lipids from the crushed linseeds was modeled using either already calibrated models of del Valle et al (Eq. 38) [47], del Valle and Aguilera (Eq. 39) [48] and Sovová et al (Eq. 40) [49] or by utilizing simpler empirical expressions of either Chrastil (Eq. 41) [50] or del Valle et al (Eq. 42) [48] where the parameters were estimated (**Table 5**). Note that Eq. (42) is based on Eq. (39) but altered so that the constants are estimated instead.

The partition equilibrium between the solid matrix and the $scCO_2$ inside the pores of the particle was described by an partition isotherm, however, described as lipids partitioning from the solid matrix into the $scCO_2$ where the maximum capacity of the solvent is described by the solubility, here denoted as c_{sat} (g / m^3) (**Table 6**). This approach has previously been utilized and proven to correctly describe the partitioning or the solute-solid interactions of lipids [13, 14].

Table 3. All of the evaluated correlations belonging to the external mass transfer resistance model class.

King et al. [38]	$Sh = 0.82Re^{0.6}Sc^{1/3}$	(21)
Puiggené et al. [39]	$Sh = 0.206Re^{0.8}Sc^{1/3}$	(22)
Tan et al. [40]	$Sh = 0.38Re^{0.38}Sc^{1/3}$	(23)
Wakao and Funazkri [41]	$Sh = 2 + 1.1Re^{0.6}Sc^{1/3}$	(24)
Estimated	$Sh = \beta_{Sh,1}Re^{\beta_{Sh,2}}Sc^{1/3}$	(25)

Table 4. All of the evaluated correlations belonging to the diffusivity model class.

Stokes-Einstein	$D_{12} = \beta_{SE}\frac{T}{\eta}$	(26)
Modified Stokes-Einstein [42]	$D_{12} = \beta_{mSE,1}\left(\frac{T}{\eta}\right)^{\beta_{mSE,2}}$	(27)
D/T-viscosity correlation [43]	$D_{12} = \beta_{DT,1}T\eta^{\beta_{DT,2}}$	(28)
Simple correlations [44]	$D_{12} = \beta_{Ma,1,1}\frac{T}{\eta} + \beta_{Ma,1,2}$	(29)
	$\frac{D_{12}}{T} = \beta_{Ma,2,2}\frac{T}{\eta} + \beta_{Ma,2,2}$	(30)
	$\ln(D_{12}) = \beta_{Ma,3,1}\ln\left(\frac{T}{\eta}\right) + \beta_{Ma,3,2}$	(31)
	$\ln\left(\frac{D_{12}}{T}\right) = \beta_{Ma,4,1}\ln\left(\frac{T}{\eta}\right) + \beta_{Ma,4,2}$	(32)
	$D_{12} = \beta_{Ma,5,1}\frac{1}{\eta} + \beta_{Ma,5,2}$	(33)
	$\ln(D_{12}) = \beta_{Ma,6,1}\ln(\eta) + \beta_{Ma,6,1}$	(34)
	$\frac{D_{12}}{T} = \beta_{Ma,7,1}\rho + \beta_{Ma,7,2}$	(35)
	$\frac{D_{12}}{T} = \beta_{Ma,8,1}\ln(\rho) + \beta_{Ma,8,2}$	(36)
	$\frac{D_{12}}{T} = \beta_{Ma,9,1}\ln(\rho) + \frac{\beta_{Ma,9,2}}{\eta}$	(37)

Table 5. All of the evaluated correlations belonging to the solubility model class. The solubility is here given in g/m^3.

Del Valle et al. [47]	$c_{sat} = 8.07\rho\left(\frac{\rho}{910}\right)^{9.59-8.45\left(\frac{\rho}{910}-1\right)-23.0\left(\frac{\rho}{910}-1\right)^2} e^{-4182\left(1-259\left(\frac{1}{T}-\frac{1}{313}\right)\right)\left(\frac{1}{T}-\frac{1}{313}\right)}$	(38)
Del Valle and Aguilera [48]	$c_{sat} = \rho^{10.742}e^{\left(-26.810-\frac{18708}{T}+\frac{2186840}{T^2}\right)}$	(39)
Sovóva et al. [49]	$c_{sat} = \rho^{1.4+0.0048\rho-0.000002\rho^2}e^{\left(-3.232-\frac{5000}{T}\right)}$	(40)
Chrastil correlation [50]	$c_{sat} = \rho^{\beta_{Chr,1}}e^{\left(\beta_{Chr,2}-\frac{\beta_{Chr,3}}{T}\right)}$	(41)
Del Valle and Aguilera correlation [48]	$c_{sat} = \rho^{\beta_{DVA,1}}e^{\left(\beta_{DVA,2}-\frac{\beta_{DVA,3}}{T}+\frac{\beta_{DVA,4}}{T^2}\right)}$	(42)

Table 6. All of the evaluated correlations belonging to the partition isotherm model class.

Linear	$c_p = K_{lin} q$	(43)
Freudlich	$c_p = K_F q^{1/n_F}$	(44)
Langmuir	$c_p = \frac{c_{sat} K_L q}{1 + K_L q}$	(45)
Redlich-Peterson	$c_p = \frac{c_{sat} K_{RP} q}{1 + K_{RP} q^{n_{RP}}}$	(46)
Toth	$c_p = \frac{c_{sat} K_T q}{(K_T + q)^{1/n_T}}$	(47)
Sips	$c_p = \frac{c_{sat} (K_S q)^{n_S}}{1 + (K_S q)^{n_S}}$	(48)

2.4. Mathematical methodologies

The partial differential equations, assuming one-dimensional symmetry, were discretized in space by the finite volume method where the control volume in the column domain and the particle domain were equally sized, respectively [51]. A two-point backward difference scheme was used for the first order differential equations and a three-point central difference scheme was used for the second order differential equations. The obtained system of ordinary differential equations (ODE) were solved using a numerical solver for stiff ODE problems using a variable order method, named *ODE15s* in MATLAB.

The extraction curve was calculated by integrating the concentration at the outlet over time (Eq. 49).

$$\hat{y} = Q \int_0^t c_b|_{z=L} dt \tag{49}$$

The cumulative extraction yield over time is what is presented throughout this work and was used in the calibration of the model structures using the experimental data in order to estimate the parameters through the inverse method.

The simplest model structures with an analytical solution were calibrated using experimental data by minimizing the root mean squared error of the calibration (RMSEC) (Eq. 50), where the minimum was found using a constrained interior-point algorithm, called *Fmincon* in MATLAB.

$$\min \sqrt{\frac{1}{N} \sum_i^N (y_i - \hat{y}_i)^2} \tag{50}$$

The parameters of the simulated models acquired by the numerical ODE solver were estimated using a population based solver. This was the preferred choice due to the induced error by numerical integration thus resulting in a noisy fitness function. But also in order to minimize the substantial risk of not finding a global minimum due to large number

of parameters to be estimated simultaneously. Thus the particle swarming optimization (PSO) algorithm was used to minimize the fitness function [52].

In order to attempt to find the most suitable model structure for both the GRM and the EHBM two optimization approaches were utilized. An overview of the methodology is given in **Fig. 2**. The optimization criterion for the model structure estimation was the same as for the model structure calibration, namely by minimizing the RMSEC according to Eq. (50). One proposed method is based on a sampling of model classes using Latin hypercube sampling (LHS), which maximizes the minimum distance in space between sampling points [53]. The best candidate model structure found in the LHS step was further optimized by evaluating all of the equations within one model class at the time. In practice subsequently after LHS step, all of the expressions describing the Nernst diffusion layer were evaluated using the currently best model structure. Then the best candidate model structure found in the previous step was used to find the expression for diffusivity yielding the lowest RMSEC. This procedure was continued until the best expression in each model class had been determined. The second method utilized a metaheuristic and population based optimizer, the genetic algorithm (GA), which was setup to handle integer problems.

Finally, the CV was performed using a simple 10-fold block CV. In order for repeated CVs to obtain comparable results between models, the stream of random numbers was standardized upon randomizing the order to experiments before performing the CV.

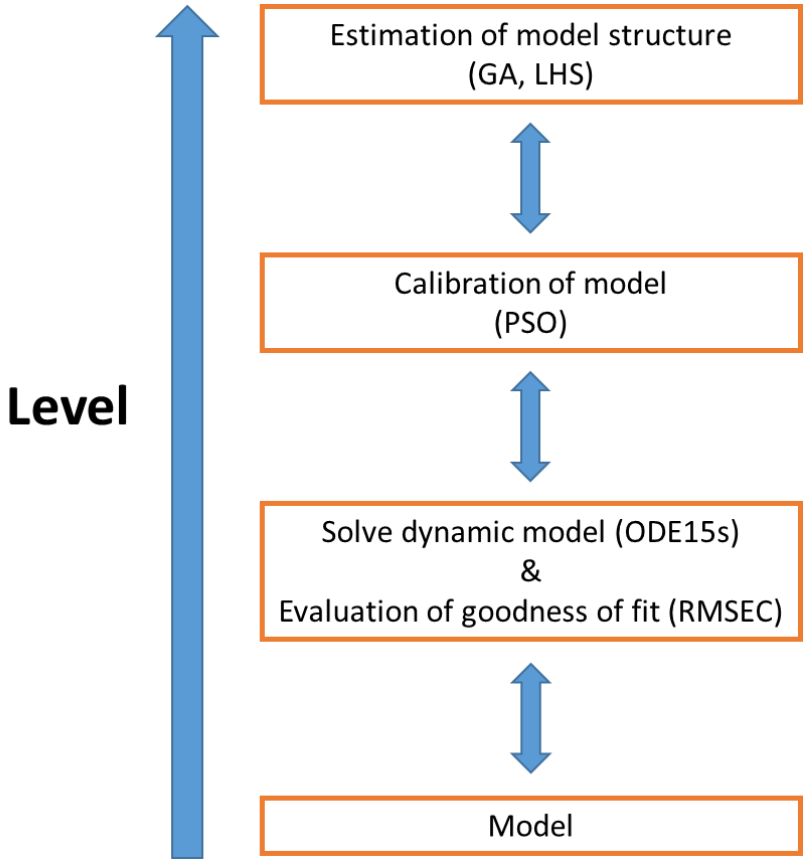

Fig. 2. Overview of the inverse modeling methodology using complete calibration for finding the final model to describe the SFE process of lipids from crushed linseeds.

3. Results and discussion

Lipids from crushed linseed were extracted under various conditions ranging from 313 to 353 K, 15 to 30 MPa and 0.5 to 1.5 mL/min in a complete full factorial design with three levels and three center points, thus resulting in 29 experiments. The extraction process was continuously monitored using an on-line ELSD, based on a previously validated method [28]. The ELSD measures the total mass of lipids in the outgoing extraction solvent with a high scan rate (>1 Hz). The extraction curves are presented in **Fig. 3** and it can be observed that there is substantial difference in extraction efficiency between the various conditions. As expected the extraction rate is substantially lower at lower densities and at the extraction condition with the lowest density nothing measureable was extracted.

The particle size of the crushed seeds was estimated by sieving and by microscopy and the mean particle diameter was 2.2 ± 0.1 mm (95% CI, n=60) and the prediction interval was 2.2 ± 0.9 mm (95% PI, n=60). Some skepticism should be added here as it is known that plant material can swell when in contact with $scCO_2$ [54].

In a previous work it was found that channeling effects were present in the extraction of lipids from linseeds, where only 55% of all the extractable compounds were acquired in the first extraction [28]. Since the same equipment, including extraction vessels and general methodology were the same and the same batch of sample was used, it was also assumed that this was the case in this work. This was taken into account in the mechanistic models and it was assumed that the formed agglomerates were evenly distributed throughout the extraction column.

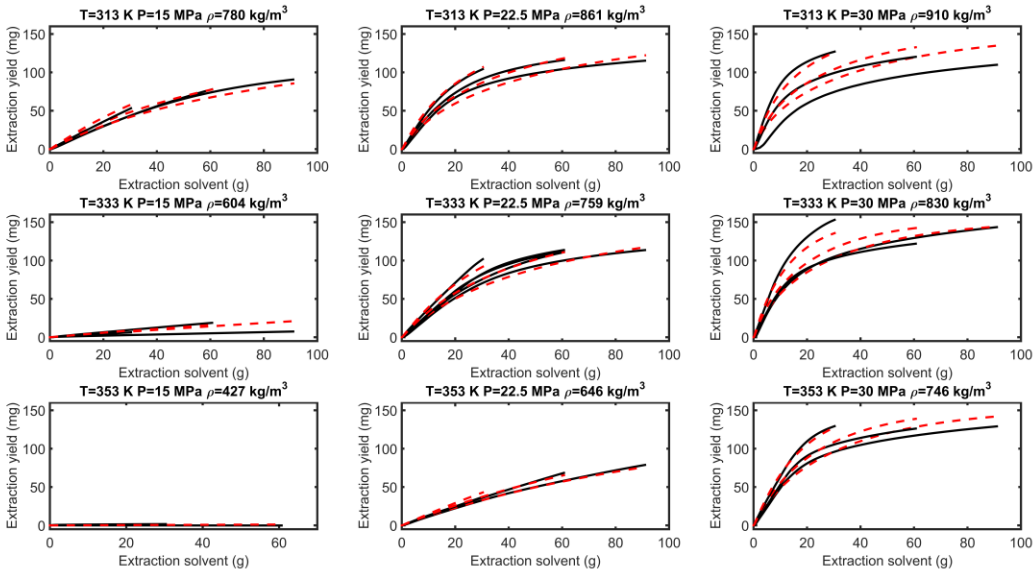

Fig. 3. Overlaid extractograms with varying flow rates (0.5, 1 and 1.5 ml/min) where the yield is plotted against the used solvent amount. The full lines represent experimental data and the dashed lines are simulated extractions using the calibrated top model structure of the GRM. Each sub-plot represents the varying temperature and pressure. The shorter lines represent the lower flow rates because of the constant extraction time.

Therefore, the cross-section area of the cylinder profile was multiplied by 0.55 to adjust for the channeling factor. This assumption may be oversimplified, but it becomes a necessity in order to model the extraction process in a manageable

manner. Furthermore, currently very little is known regarding this phenomenon and only a few studies in the literature have reported its presence, e.g. Abrahamsson et al. [28].

The measurement of fit for the calibration was the RMSEC and the root mean square error of the cross-validation (RMSECV) was used a measurement for the CV. The RMSEC was used as the minimization criteria for all of the numerical optimization methods. As the DOE involved three replicates in the center point (T=333 K, P=22.5 Mbar, Q=1 mL/min) the root mean square error (RMSE) could be estimated from these continuous measurements. The mean RMSE throughout the whole extraction process was estimated to 2.04 mg, whereof the average final yield was 112.20 mg. Although it might be faulty to assume homoscedasticity over the entire design space, it does give an indication of how well a model can perform in relation to incorporating random variation. In practice it is sound to assume that a model with a RMSEC of 2 mg is not comparably worse than a model of 0.5 mg. In the latter scenario over-fitting might be anticipated.

3.1. Optimization of numerical solvers

Several techniques and algorithms were evaluated for the minimization of the fitness function used for estimating parameters for the various models. For the simple models with an analytical solution a gradient based numerical solver was efficient. However, for the mechanistic models with more parameters to be fitted, gradient based solvers and also solvers based on mesh-adaptive direct search algorithms were not able to converge towards a global minimum. Therefore, both GA and PSO were evaluated and it was found that in general the PSO algorithm required less than half of the function evaluations needed compared to GA in order to achieve the same results (data not shown). The simulations were also optimized in terms of mesh of the finite volumes and the numerical solvers in order to ensure good enough accuracy of the numerical ODE solver. It was found that 30 grid points in the column domain and 10 in the particle domain was enough if an algebraic expression was applied extrapolating the concentration at the particle surface from the most outer grid point in the particle and the column domain, instead of just using the most outer grid point.

3.2. Single calibration models

Parameters are usually estimated by model calibration using one experiment at the time, thus generating one set of parameters for each experiment. Six different models were calibrated using this particular approach, namely the one-term exponential with one parameter (Eq. 1), two parameters (Eq. 2), the hot ball model (Eq. 3), the DLT model (Eq. 4), a mechanistic model (Eqs. 6-13) and a mechanistic model with a distribution ratio parameter (Eqs. 14-15). In the two mechanistic models the initial values of the particles were set to the initial solute concentration.

Interestingly the purely empirical models had a much better fit than the semi-empirical or the mechanistic models (**Table 7**). The average RMSEC of the one parameter one-term exponential model was 4.37 mg, 1.16 mg for the two parameter one-term exponential model, 7.55 mg for the hot ball model, 4.69 mg for the DLT model, 2.10 mg and 2.10 mg for the mechanistic without and with a partition ratio parameter, respectively. The one parameter exponential, the hot ball model and the DLT model all have one parameter which is estimated using model calibration. Out of these the empirical equation performed best in regards of RMSEC.

Table 7. Extraction conditions of all the performed experiments and the results of the single calibrations of various models.

Extraction conditions				One parameter exponential model		Two parameter exponential model			DLT model		Hot ball model		Mechanistic model			Mechanistic model with a distribution constant			
Pressure (MPa)	Temperature (K)	Density (kg/m^3)	Flow rate (mL/min)	k (1/s)	RMSEC (mg)	H	k (1/s)	RMSEC (mg)	β_{DLT}	RMSEC (mg)	D_e (m^2/s)	RMSEC (mg)	D_e (m^2/s)	k_f (m/s)	RMSEC (mg)	D_e (m^2/s)	k_f (m/s)	k_D	RMSEC (mg)
15	313	780	0.5	9.90×10^{-5}	0.86	4.7279	1.89×10^{-5}	0.10	1.02×10^{-4}	0.58	1.88×10^{-9}	6.49	6.39×10^{-7}	4.18×10^{-8}	0.79	2.68×10^{-9}	6.97×10^{-8}	1.657	0.79
15	313	780	1	1.66×10^{-4}	0.86	1.3240	1.18×10^{-4}	0.43	1.70×10^{-4}	0.30	4.81×10^{-9}	9.02	9.42×10^{-8}	7.03×10^{-8}	0.99	1.17×10^{-9}	2.17×10^{-8}	0.305	0.99
15	313	780	1.5	2.31×10^{-4}	2.35	0.7626	3.43×10^{-4}	1.10	2.38×10^{-4}	2.79	8.64×10^{-9}	8.80	7.83×10^{-11}	1.32×10^{-7}	1.50	8.30×10^{-6}	4.85×10^{-6}	45.922	1.78
15	333	604	0.5	1.05×10^{-5}	0.02	9.9987	1.04×10^{-6}	0.01	1.07×10^{-5}	0.04	9.97×10^{-24}	2.61[a]	2.61×10^{-7}	4.34×10^{-9}	0.02	2.44×10^{-7}	1.63×10^{-10}	0.038	0.02
15	333	604	1	3.22×10^{-5}	0.07	0.7594	4.29×10^{-5}	0.05	3.29×10^{-5}	0.21	2.19×10^{-10}	2.74	3.38×10^{-11}	1.41×10^{-8}	0.06	7.41×10^{-11}	2.08×10^{-8}	1.514	0.07
15	333	604	1.5	1.27×10^{-5}	0.21	0.1127	1.32×10^{-4}	0.12	1.30×10^{-5}	0.27	2.58×10^{-12}	2.31	2.78×10^{-13}	1.06×10^{-8}	0.12	1.26×10^{-13}	6.41×10^{-9}	0.071	0.12
15	353	427	0.5	3.45×10^{-6}	0.33	0.0092	1.16×10^{-3}	0.11	3.52×10^{-6}	0.35	1.60×10^{-24}	3.83[a]	3.10×10^{-14}	1.48×10^{-8}	0.33	2.98×10^{-14}	1.31×10^{-6}	55.627	0.33
15	353	427	1	4.83×10^{-14}	0.09	0.0022	3.66×10^{-10}	0.09	1.00×10^{-10}	0.09	7.04×10^{-24}	5.12[a]	1.00×10^{-18}	1.00×10^{-14}	0.09[a]	1.00×10^{-16}	1.00×10^{-10}	99.974	0.09[a]
15	353	427	1.5	1.35×10^{-6}	0.07	0.0050	4.83×10^{-4}	0.03	1.38×10^{-6}	0.08	3.22×10^{-24}	4.60[a]	1.97×10^{-13}	5.97×10^{-10}	0.07	1.06×10^{-14}	9.96×10^{-6}	0.001	0.07
22.5	313	861	0.5	2.80×10^{-4}	1.85	0.8618	3.50×10^{-4}	1.13	2.88×10^{-4}	2.25	1.18×10^{-8}	10.24	4.38×10^{-8}	1.24×10^{-7}	1.13	9.18×10^{-7}	7.10×10^{-9}	0.058	1.13
22.5	313	861	1	3.95×10^{-4}	7.21	0.7319	7.30×10^{-4}	0.73	4.07×10^{-4}	8.15	2.03×10^{-8}	7.30	5.71×10^{-11}	4.39×10^{-7}	2.54	5.70×10^{-11}	6.42×10^{-7}	1.456	2.54
22.5	313	861	1.5	4.25×10^{-4}	11.83	0.6767	1.03×10^{3}	1.64	4.38×10^{-4}	12.89	2.27×10^{-8}	5.81	4.29×10^{-11}	1.11×10^{-6}	4.16	4.29×10^{-11}	3.03×10^{-6}	2.664	4.16
22.5	333	759	0.5	2.28×10^{-4}	3.08	2.5412	7.48×10^{-5}	0.24	2.35×10^{-4}	2.54	8.35×10^{-9}	12.56	5.45×10^{-8}	9.91×10^{-8}	3.40	5.15×10^{-9}	1.46×10^{-7}	1.467	3.40
22.5	333	759	1	3.13×10^{-4}	2.06	0.8672	3.91×10^{-4}	1.13	3.22×10^{-4}	2.56	1.42×10^{-8}	10.53	8.21×10^{-10}	1.43×10^{-7}	1.10	4.33×10^{-9}	4.25×10^{-8}	0.307	1.10
22.5	333	759	1	3.41×10^{-4}	3.20	0.8916	4.10×10^{-4}	2.76	3.51×10^{-4}	3.24	1.61×10^{-8}	11.94	1.06×10^{-7}	1.50×10^{-7}	2.55	3.56×10^{-8}	9.42×10^{-8}	0.624	2.56
22.5	333	759	1	3.37×10^{-4}	3.53	0.8230	4.66×10^{-4}	2.03	3.47×10^{-4}	3.96	1.59×10^{-8}	10.53	4.74×10^{-9}	1.50×10^{-7}	2.42	2.67×10^{-6}	2.88×10^{-10}	0.002	2.43
22.5	333	759	1.5	3.73×10^{-4}	6.60	0.7331	6.72×10^{-4}	1.54	3.85×10^{-4}	7.39	1.87×10^{-8}	8.25	6.14×10^{-11}	3.45×10^{-7}	3.14	6.14×10^{-11}	6.99×10^{-6}	18.675	3.14
22.5	353	646	0.5	6.56×10^{-5}	0.45	9.1417	6.64×10^{-6}	0.10	6.73×10^{-5}	0.24	8.73×10^{-10}	4.62	2.19×10^{-6}	2.75×10^{-8}	0.38	1.11×10^{-9}	7.45×10^{-8}	2.690	0.38
22.5	353	646	1	1.36×10^{-4}	0.84	1.6629	7.57×10^{-5}	0.24	1.39×10^{-4}	0.69	3.37×10^{-9}	7.80	2.35×10^{-9}	5.74×10^{-8}	0.99	4.06×10^{-6}	5.76×10^{-10}	0.010	0.99
22.5	353	646	1.5	1.73×10^{-4}	0.48	0.8963	1.99×10^{-4}	0.25	1.78×10^{-4}	1.00	5.24×10^{-9}	8.12	3.87×10^{-6}	7.33×10^{-8}	0.22	3.44×10^{-10}	1.40×10^{-7}	1.819	0.22
30	313	910	0.5	4.81×10^{-4}	7.34	0.7892	7.96×10^{-4}	1.54	4.98×10^{-4}	8.28	2.69×10^{-8}	8.55	8.08×10^{-11}	5.22×10^{-7}	2.96	8.01×10^{-11}	4.60×10^{-6}	7.373	2.97
30	313	910	1	4.60×10^{-4}	12.20	0.6962	1.09×10^{3}	2.15	4.75×10^{-4}	13.39	2.54×10^{-8}	5.12	4.55×10^{-11}	1.67×10^{-6}	3.44	4.60×10^{-11}	6.07×10^{-7}	0.390	3.44
30	313	910	1.5	3.72×10^{-4}	10.14	0.6593	8.84×10^{-4}	2.20	3.83×10^{-4}	11.04	1.87×10^{-8}	6.41	3.95×10^{-11}	6.70×10^{-7}	4.02	3.95×10^{-11}	1.16×10^{-8}	0.017	4.02
30	333	830	0.5	5.96×10^{-4}	2.75	1.0644	5.29×10^{-4}	1.99	6.21×10^{-4}	1.21	3.65×10^{-8}	15.30	5.23×10^{-8}	2.85×10^{-7}	5.29	6.97×10^{-9}	9.96×10^{-6}	24.605	4.95
30	333	830	1	4.86×10^{-4}	12.50	0.7102	1.12×10^{3}	1.82	5.03×10^{-4}	13.65	2.74×10^{-8}	6.09	5.12×10^{-11}	1.43×10^{-6}	4.35	5.12×10^{-11}	2.15×10^{-7}	0.154	4.35
30	333	830	1.5	6.94×10^{-4}	10.76	0.8197	1.19×10^{3}	3.05	7.25×10^{-4}	12.24	4.34×10^{-8}	5.70	1.01×10^{-10}	1.15×10^{-6}	2.58	1.01×10^{-10}	1.11×10^{-6}	0.967	2.58
30	353	746	0.5	4.12×10^{-4}	2.51	1.0544	3.77×10^{-4}	2.35	4.26×10^{-4}	1.83	2.15×10^{-8}	14.08	7.18×10^{-7}	1.87×10^{-7}	3.16	7.52×10^{-7}	2.12×10^{-8}	0.114	3.16
30	353	746	1	4.99×10^{-4}	9.84	0.7586	9.37×10^{-4}	2.42	5.17×10^{-4}	10.79	2.83×10^{-8}	8.21	7.26×10^{-11}	6.36×10^{-7}	4.72	7.26×10^{-11}	7.26×10^{-6}	10.160	4.73
30	353	746	1.5	5.50×10^{-4}	12.70	0.7422	1.18×10^{-3}	2.43	5.70×10^{-4}	13.96	3.22×10^{-8}	6.19	6.24×10^{-11}	1.41×10^{-6}	4.41	6.24×10^{-11}	2.66×10^{-9}	0.002	4.41
				Mean RMSEC	4.37		Mean RMSEC	1.16	Mean RMSEC	4.69	Mean RMSEC	7.55		Mean RMSEC	2.10			Mean RMSEC	2.10

[a] Parameters could not be estimated properly as they were approaching extreme values.

These models were outperformed by the two and three parameter models. Interestingly, the one-term exponential with two parameters had the lowest RMSEC. Therefore, a more complex model does not ensure a better fit to experimental data, although it can easily be argued that a mechanistic model will have more physical meaning and give additional information about the underlying processes taking place in the SFE of lipids.

There is an abundance of examples in the literature where the diffusion constant has been determined using the single calibration approach [7]. Quite often the number of experiments are relatively small in number and therefore it can be difficult to judge whether estimated diffusion constants vary in a manner which makes physical sense. Interestingly, it can be noted that for the calibration of the hot ball model, DLT model, and the two versions of the mechanistic model, the estimated diffusivities or the related parameter varied much more than what could be expected. Furthermore, the estimated diffusion constant or the related estimated parameter in the DLT model, β_{DLT}, did not vary in a manner which could be considered systematic (**Table 7**). These observations give further weight to the argument that individual extraction curves do not contain enough unique information to be able to correctly estimate parameters of physical meaning [14].

3.3. Complete calibration models

One approach to deal with the potentially problematic challenges in correctly estimating the true physical properties and mass transfer phenomena due to sparse information in each experiment is to use more experiments for each model calibration. To obtain a larger dataset of several extractions with many measurements at time intervals during each extraction is usually time consuming. However, by using on-line detection the effort is minimized and many extraction curves can be obtained swiftly [28]. By having more experimental data per parameter estimated, the over-fitting and thus the instability of the parameter estimation could possibly be reduced.

Therefore, a methodology was set up to estimate both the model structure and to estimate its unknown parameters by model calibration using the whole dataset of 29 experiments at various SFE conditions. Consequently, a model is obtained which has predictability over the whole design space of experiments. The model structure describes and correlates the physical properties and mass transfer phenomena including diffusivity, the Nernst diffusion layer, solubility and the partitioning of lipids between the $scCO_2$ and the solid matrix. The parameters of the model structures were estimated by minimizing the overall RMSEC. Here two general approaches were utilized to inversely model the SFE process, namely the EHBM and the GRM

The model classes and their contained equations can be seen in **Fig. 1**. Since one equation is chosen from each class to form a candidate model structure, the construction of the model structures becomes a combinatorial problem. The correlations included in the model classes have varying number of parameters which need to be estimated. For the EHBM correlations for the Nernst diffusion layer, the external diffusivity, the intra-particle diffusivity and the solubility are used. This results in 1120 possible combinations of equations to form a model structure. In the GRM the external diffusivity and the intra-particle diffusivity are not estimated independently. Instead the binary diffusivity is corrected with the particle porosity factor. The GRM also utilize a partition isotherm expression to describe the partitioning of the lipids between the $scCO_2$ in the particle pores and the solid matrix. This yields 1716

possible combinations of model structures for the GRM. To evaluate all of the candidate model structures would become too expensive in terms of computational power.

Therefore, optimization of the model structure was performed using two different approaches by either employing GA or by evaluating one model class at the time. The GA is known to be computationally heavy in terms of the many function evaluations usually needed to converge towards a solution. However, it is also known that combinatorial optimization problems are very difficult to handle and to ensure that a global optimum is found an exhaustive search is needed [55]. Because of the large number of possible combinations and the computationally expensive fitness function due to the many simulations performed at each iteration it may not be feasible. Initiating with a LHS step and subsequently optimizing each class one at the time was also evaluated as a second alternative.

Upon estimating the model structure of the EHBM, a minimum was found using GA after 127 fitness function evaluations giving a mean RMSEC of 6.47 mg (**Table A.1**). The proposed method of an initial LHS step before optimizing the combinations by one model class at the time, performed 33 function calls and obtained a calibrated model resulting in a mean RMSEC of 6.43 mg (**Table 8**).

While for the model structure optimization of the GRM, the GA converged to a solution after 233 fitness function evaluations with the best model giving a mean RMSEC of 4.80 mg (**Table 9**). By evaluating one model class at the time, 42 fitness function evaluations were made before finding a model structure which gave a mean RMSEC of 5.29 mg (**Table A.2**). For comparison, the worst GRM model structure resulted in a mean RMSEC of about 50 mg.

It is clear that GA will perform more fitness function evaluations before converging towards a solution, although this will depend on settings such as mutation factor, elite count *etc* [55]. However, if GA is a too expensive option in terms of computational power, then the proposed algorithm is efficient at obtaining a good estimate of the model structure from the experimental data. In the optimization of the model structure for the EHBM the GA performed slightly worse out of the two methods although the differences in RMSEC were relatively small. However, for the GRM the GA found a model structure which had a lower RMSEC in comparison, although at the cost of a substantially larger number of fitness function evaluations.

Table 8. The 10 best-fit candidate model structures for the EHBM using LHS and optimizing one model class at the time. Complete calibrations were performed.

Ext. mass trans. res.	Ext. diffusivity	Diffusivity	Solubility	RMSEC (mg)
King et al.	SE	Ma7	Sovová et al.	6.43
King et al.	Const. (Est.)	Ma7	Sovová et al.	6.48
Tan et al.	Const. (Est.)	Ma7	Sovová et al.	6.48
King et al.	SE	Ma3	Sovová et al.	6.49
King et al.	SE	Ma8	Sovová et al.	6.50
Est.	Const. (Est.)	Ma7	Sovová et al.	6.51
Wakao & Funazkri	Const. (Est.)	Ma7	Sovová et al.	6.52
King et al.	SE	Ma9	Sovová et al.	6.59
King et al.	SE	Ma4	Sovová et al.	6.61
Puiggené et al.	Const. (Est.)	Ma7	Sovová et al.	6.62

Table 9. The 15 best-fit candidate model structures for the GRM using GA. Complete calibrations were performed.

Ext. Mass Tans. Res.	Diffusivity	Solubility	Partition isotherm	RMSEC (mg)
Est.	Ma6	Sovová et al.	Toth	4.80
Est.	Ma7	Sovová et al.	Toth	5.71
Est.	Ma2	Sovová et al.	Toth	6.03
Est.	Ma9	Sovová et al.	Toth	6.04
Est.	Ma1	Sovová et al.	Toth	6.04
Est.	Ma3	Sovová et al.	Toth	6.09
Tan et al.	Ma2	Sovová et al.	Toth	6.12
Tan et al.	Ma1	Sovová et al.	Toth	6.18
Wakao & Funazkri	Ma2	Sovová et al.	Toth	6.11
King et al.	Ma1	Sovová et al.	Toth	6.14
Wakao & Funazkri	Ma3	Sovová et al.	Toth	6.12
Puiggené et al.	Ma2	Sovová et al.	Toth	6.15
King et al.	Ma3	Sovová et al.	Toth	6.15
Wakao & Funazkri	Ma1	Sovová et al.	Toth	6.18
King et al.	Ma2	Sovová et al.	Toth	6.21

More evaluations are needed to definitely confirm which method is more efficient as it is probably highly dependent on the start point.

Upon inspecting the top five candidate model structures from using each method for both the EHBM and the GRM, it can be observed that the solubility model of Sovová is the top candidate in all instances and exclusively chosen upon utilizing GA. Thereby it can be concluded that the Sovová solubility correlation outperforms the other expressions.

Furthermore, for the model structure of the GRM, the Toth partition isotherm was exclusively found among the top candidates as the most suitable expression from the partition isotherm model class. No apparent trend could be found upon investigating the top candidate model structures in terms of the model classes of diffusivity and the Nernst diffusion layer. It could be argued that the expressions are all capable of explaining the effects of these phenomena, at least within the experimental design space. Therefore, it might be recommended that efforts should be directed towards finding appropriate expressions describing the partitioning and the solubility, rather than mass transfer by diffusion.

3.4. Cross-validation and uncertainty analysis

In order to estimate the prediction power of the selected model structures a CV was performed. A 10-fold blocked CV was used and the estimated model parameters were obtained for each fold in order to get an indication of the uncertainty of the parameter estimation (**Table 10**). For proper evaluation of the estimated parameters a jack-knifing or a bootstrapping methodology is advisable. However, due to the relatively computationally heavy model calibrations and the main interest of predictability and the over-fitting of the models, a CV methodology was chosen.

Table 10. Results from the CV of the top four candidate model structures for the GRM and the top candidate of the EHBM.

Modeling approach	Ext. mass. trans. res.	Diffusivity in particle	Solubility	Partition isotherm	RMSEC (mg)	RMSECV (mg)	Median (min, max)
GRM	Est.	Ma6	Sovová et al.	Toth	4.77	5.22	$\beta_{Sh,1}$ = 0.90 (0.60, 0.98) $\beta_{Sh,2}$ = 0.87 (0.67, 0.96) $\beta_{Ma,6,1}$ = -3.28 (-4.37, -2.58) $\beta_{Ma,6,2}$ = -45.2 (-54.9, -40.4) K_T = 2.58 (1.55, 3.72) n_T = 3.72 (2.03, 6.97) ε_p = 0.0055 (0.0051, 0.37) k_f = 1.02×10^{-4} (9.58×10^{-5}, 1.00×10^{-4})
GRM	Const. (Est.)	Ma6	Sovová et al.	Toth	5.00	5.44	$\beta_{Ma,6,1}$ = -4.40 (-4.50, -3.02) $\beta_{Ma,6,2}$ = -57.1 (-60, -42.5) K_T = 2.27 (1.59, 4.88) n_T = 5.97 (2.0, 7.50) ε_p = 0.015 (0.006, 0.31) $\beta_{Sh,1}$ = 0.12 (0.10, 0.98) $\beta_{Sh,2}$ = 0.70 (0.63, 0.98)
GRM	Est.	Ma7	Sovová et al.	Toth	5.73	6.39	$\beta_{Ma,7,1}$ = -5.38×10^{-16} (-1.04×10^{-12}, -1.03×10^{-18}) $\beta_{Ma,7,2}$ = 1.69×10^{-12} (1.09×10^{-12}, 9.99×10^{-10}) K_T = 44 (3, 200) n_T = 4.1 (2.3, 7.3) ε_p = 0.68 (0.11, 0.70)
GRM	Est.	Ma2	Sovová et al.	Toth	6.03	6.51	$\beta_{Sh,1}$ = 0.61 (0.15, 0.97) $\beta_{Sh,2}$ = 0.98 (0.61, 0.98) $\beta_{Ma,2,1}$ = 2.84×10^{-15} (1.82×10^{-16}, 1.01×10^{-14}) $\beta_{Ma,2,2}$ = 2.03×10^{-17} (2.72×10^{-19}, 1.03×10^{-15}) K_T = 2.9 (2.1, 67)

Modeling approach	Ext. mass. trans. res.	Diffusivity in particle	Solubility	Partition isotherm	RMSEC (mg)	RMSECV (mg)	Median (min, max)
EHBM	King et al. & SE	Ma7	Sovová et al.	-	6.55	6.54	n_T = 3.6 (2.12, 6.6) ε_p = 0.34 (0.093, 0.69) β_{SE} = 1.2×10^{-12} (7.5×10^{-14}, 7.0×10^{-12}) $\beta_{Ma,7,1}$ = -4.6×10^{-17} (-2.4×10^{-16}, -1×10^{-17}) $\beta_{Ma,7,2}$ = 1.7×10^{-13} (1.3×10^{-13}, 3.3×10^{-13})

The RMSEC values vary slightly between the model structure estimation procedure and the CV because the RMSEC in the latter case is based on the mean RMSEC of the CV.

The RMSEC and the RMSECV for some of the top candidate model structures did not differ substantially. For example, the model structure with the lowest RMSEC, obtained using the GA for the GRM, had a RMSEC of 4.77 mg and a RMSECV of 5.22 mg. The model calibration of this candidate model structure involved the simultaneous estimation of seven model parameters. By having a large number of estimated parameters the risk of over-fitting increases. However, the low RMSEC and the RMSECV indicate a good fit for both the calibration and the predictability of the model. Therefore, it can be concluded that over-fitting which reduce predictability does not take place. The same trend was observed for the other model structures which were evaluated by CV (**Table 10**). Nonetheless, this is an important part of the inverse modeling approach as good fit of the calibration does not necessarily ensure good predictability.

Due to the nature of the CV the parameters of each fold are also obtained. Although they do not estimate an interval of the estimated parameters, an indication can be given regarding the stability of the parameter estimation. Upon investigating the parameters of each fold for the various CV performed, it was noticed that in general the estimated parameters where the values were deviating only did so for one or two of the folds. The spread of the parameters did not indicate a normal distribution and therefore the median and the minimum and the maximum values are presented. The precision of the parameter estimation was particularly poor for the external mass transfer resistance correlation and the factor relating to the porosity. Whilst for the other parameters the maximum and minimum values were relatively close to the median value, but yet with a substantial spread. The optimum model structure found for the EHBM had a much smaller interval of estimated model coefficients.

At this point, it should also be mentioned that it would be preferable to utilize the RMSECV rather than the RMSEC for the model structure estimation. However, it would increase the computational time with a factor equal to the number of folds of the CV.

4. Conclusions

Lipids from crushed linseeds were extracted using SFE with an on-line ELSD. From the generated data empirical, semi-empirical and mechanistic models were evaluated. Initially the model parameters were estimated using single calibrations, which is the usual procedure applied in the literature. It was found that the purely empirical models had a better fit in terms of RMSEC compared to the more complex models. It was also observed that the estimated parameters corresponding to for example the diffusivity had a large deviation and did not vary in a systematical manner. This proves that single extraction curves may not contain enough relevant information to estimate physical parameters as has previously been discussed [14].

By performing complete calibrations, including all of the 29 experiments performed, a more robust parameter estimation was obtained (**Table 11**). Two approaches were utilized, namely the GRM and the proposed and slightly more simple EHBM. However, due to the many estimated parameters, efforts were made to optimize the numerical solvers to reduce computational time and yet obtaining correct solutions. PSO was found to be a good option for model calibrations with many unknown parameters in the model structure.

In order to estimate the model structure of the GRM and the EHBM, two different algorithms were used – GA and a proposed method of optimizing one model class at the time after a LHS step. A substantial reduction of model class evaluations compared to evaluating all possible combinations of correlations was obtained using all of the methods. However, the GA required more iterations than the proposed LHS method before converging to a solution. For the GRM the GA performed substantially better. The best-fit model of the EHBM gave a RMSEC of 6.22 mg and the best model of GRM gave a RMSEC of 4.80 mg (**Fig. 3**). This should be compared with the RMSE of repeated measurements which was estimated to 2.04 mg. Thus it can be concluded that the proposed models have a good fit to the experimental data.

For both the EHBM and the GRM the Sovová et al. [49] solubility expression almost exclusively found among all of the top candidate model structures. The same observation was made for the Toth partition isotherm in the GRM. No specific expression describing diffusion mass transfer was retained in a similar manner within the candidate model structures. Furthermore, the less good precision of the parameter estimation indicates that the experiments may still lack information to fully discriminate between expressions describing diffusivity.

In order to ensure good predictability of the models, some of the best model structures were validated by CV. The proposed model structure for the GRM gave a RMSEC of 4.80 mg and a RMSECV of 5.22 mg. It can finally be concluded that in this work is a proposed methodology for inverse modeling ranging from data acquisition to validation.

Table 11. Overview of the properties of the $scCO_2$ and the mass transfer coefficients at the conditions of each of the experiments performed. The mass transfer properties were obtained using the complete calibration of the GRM. The model structure was the same as the best found candidate using GA. An estimation for the mass transfer resistance was used, the empirical relationship denoted Ma7 was used for the diffusivity, the Sovová solubility model was employed and the particle porosity factor was estimated. In the calibration of the model the Toth partition isotherm was utilized.

Pressure (MPa)	Temperature (K)	Flow rate (mL/min)	Density ($kg/m^{3)}$	Viscosity (Pa s)	Diffusivity (m^2/s)	Ext. mass trans. res. (m/s)	Solubility (g/m^3)	RMSEC (mg)
15	313	0.5	780	6.77×10^{-5}	1.11×10^{-6}	3.64×10^{-3}	1.05×10^{3}	4.40
15	313	1	780	6.77×10^{-5}	1.11×10^{-6}	3.64×10^{-3}	1.05×10^{3}	3.69
15	313	1.5	780	6.77×10^{-5}	1.11×10^{-6}	3.64×10^{-3}	1.05×10^{3}	4.60
15	333	0.5	604	4.61×10^{-5}	3.90×10^{-6}	9.03×10^{-3}	1.01×10^{2}	1.45
15	333	1	604	4.61×10^{-5}	3.90×10^{-6}	9.03×10^{-3}	1.01×10^{2}	1.62
15	333	1.5	604	4.61×10^{-5}	3.90×10^{-6}	9.03×10^{-3}	1.01×10^{2}	7.87
15	353	0.5	427	3.25×10^{-5}	1.23×10^{-5}	1.95×10^{-2}	3.67	0.14
15	353	1	427	3.25×10^{-5}	1.23×10^{-5}	1.95×10^{-2}	3.67	0.93
15	353	1.5	427	3.25×10^{-5}	1.23×10^{-5}	1.95×10^{-2}	3.67	0.76
22.5	313	0.5	861	8.27×10^{-5}	5.77×10^{-7}	2.23×10^{-3}	3.55×10^{3}	2.40
22.5	313	1	861	8.27×10^{-5}	5.77×10^{-7}	2.23×10^{-3}	3.55×10^{3}	3.04
22.5	313	1.5	861	8.27×10^{-5}	5.77×10^{-7}	2.23×10^{-3}	3.55×10^{3}	4.88
22.5	333	0.5	759	6.50×10^{-5}	1.27×10^{-6}	4.01×10^{-3}	1.92×10^{3}	4.02
22.5	333	1	759	6.50×10^{-5}	1.27×10^{-6}	4.01×10^{-3}	1.92×10^{3}	2.08
22.5	333	1	759	6.50×10^{-5}	1.27×10^{-6}	4.01×10^{-3}	1.92×10^{3}	5.13
22.5	333	1	759	6.50×10^{-5}	1.27×10^{-6}	4.01×10^{-3}	1.92×10^{3}	3.95
22.5	333	1.5	759	6.50×10^{-5}	1.27×10^{-6}	4.01×10^{-3}	1.92×10^{3}	3.02
22.5	353	0.5	646	5.14×10^{-5}	2.74×10^{-6}	6.98×10^{-3}	5.63×10^{2}	3.84
22.5	353	1	646	5.14×10^{-5}	2.74×10^{-6}	6.98×10^{-3}	5.63×10^{2}	1.16
22.5	353	1.5	646	5.14×10^{-5}	2.74×10^{-6}	6.98×10^{-3}	5.63×10^{2}	1.09
30	313	0.5	910	9.38×10^{-5}	3.80×10^{-7}	1.63×10^{-3}	6.73×10^{3}	7.14
30	313	1	910	9.38×10^{-5}	3.80×10^{-7}	1.63×10^{-3}	6.73×10^{3}	7.08
30	313	1.5	910	9.38×10^{-5}	3.80×10^{-7}	1.63×10^{-3}	6.73×10^{3}	20.03
30	333	0.5	830	7.68×10^{-5}	7.34×10^{-7}	2.67×10^{-3}	5.90×10^{3}	11.18
30	333	1	830	7.68×10^{-5}	7.34×10^{-7}	2.67×10^{-3}	5.90×10^{3}	13.97
30	333	1.5	830	7.68×10^{-5}	7.34×10^{-7}	2.67×10^{-3}	5.90×10^{3}	2.45
30	353	0.5	746	6.38×10^{-5}	1.35×10^{-6}	4.18×10^{-3}	3.59×10^{3}	3.10
30	353	1	746	6.38×10^{-5}	1.35×10^{-6}	4.18×10^{-3}	3.59×10^{3}	7.35
30	353	1.5	746	6.38×10^{-5}	1.35×10^{-6}	4.18×10^{-3}	3.59×10^{3}	8.55

Acknowledgements

This research was supported by the Swedish Research Council Formas (229-2009-1527) and the Swedish Research Council VR (2010-5439, 2010-333, 2013-4356, 2014-4052).

Nomenclature

A	Particle surface area (m^2)
c_b	Solute concentration in the bulk fluid (g/m^3)
c_{init}	Initial solute concentration (g/m^3)
c_p	Solute concentration in the particle (g/m^3)
c_s	Solute concentration at the particle surface (g/m^3)
c_{sat}	Solute concentration at saturation (g/m^3)
D_{12}	Binary diffusion coefficient (m^2/s)
$D_{12,\,ext}$	External binary diffusion coefficient in the bulk fluid (m^2/s)
D_e	Effective diffusion coefficient (m^2/s)
D_p	Particle diameter (m)
h	Diffusion layer thickness (m)
H	Henry's constants
k	Kinetic constant (1/s)
K_D	Partition ratio
k_f	Film mass transfer (m/s)
K_{lin}	Linear isotherm constant
K_F	Freudlich isotherm constant
K_L	Langmuir isotherm constant
K_{RP}	Redlich–Peterson isotherm constant
K_T	Toth isotherm constant (g/m^3)
K_S	Sips isotherm model constant
L	Length of the extraction vessel (m)
m	Extracted mass (g)
m_0	Extractable mass (g)
Ma1 – Ma9	Simple correlations for estimating the diffusivity given by Magalhães et al.[44]
n_F	Adsorption intensity

n_{RP}	Redlich-Peterson isotherm exponent
n_T	Toth isotherm exponent
n_S	Sips isotherm exponent
P	Pressure (MPa)
Q	Volumetric flow rate (m^3/s)
q	Solute concentration in the solid matrix (g/m^3)
Re	Dimensionless Reynolds number
r_p	Radial distance in particle (m)
r_s	Solute radius (m)
R_p	Particle radius (m)
Sc	Dimensionless Schmidt number
Sh	Dimensionless Sherwood number
t	Extraction time (s)
T	Temperature (K)
u_{lin}	Superficial linear velocity (m/s)
V	Void volume in extraction vessel (m^3)
y	Measured yield (g)
$\hat{y}$	Predicted yield (g)
z	Axial position along the packed bed (m).
$\beta_{Chr,i}$	Estimated constants of the Chrastil relationship
β_{DLT}	Estimated mass transfer constant of the DLT model (m^3/s)
$\beta_{DT,i}$	Estimated constants of the *D/T*-viscosity correlation
$\beta_{DVA,i}$	Estimated constants of the del Valle and Aguilera relationship
$\beta_{Ma,i,j}$	Estimated constants of Eqs. (33)-(41)
$\beta_{mSE,i}$	Estimated constants of Eqs. (30)-(31)
β_{SE}	Estimated combined constant of the Stokes-Einstein equation ($m\,kg / s^2\,K$)
$\beta_{Sh,\,i}$	Estimated constants for estimating the Sherwood number
ε_c	Void fraction of the column

ε_p	Porosity of the particle
η	Viscosity of the $scCO_2$ (Pa s).
ρ	Density of the CO_2 (kg / m^3)

References

[1] T. Clifford, Fundamentals of supercritical fluids, Oxford University Press, New York, 1999.

[2] C. Crampon, O. Boutin, E. Badens, Supercritical carbon dioxide extraction of molecules of interest from microalgae and seaweeds, Industrial and Engineering Chemistry Research, 50 (2011) 8941-8953.

[3] C.G. Pereira, M.A.A. Meireles, Supercritical fluid extraction of bioactive compounds: Fundamentals, applications and economic perspectives, Food and Bioprocess Technology, 3 (2010) 340-372.

[4] D. García-Rodríguez, A.M. Carro-Díaz, R.A. Lorenzo-Ferreira, Supercritical fluid extraction of polyhalogenated pollutants from aquaculture and marine environmental samples: A review, Journal of Separation Science, 31 (2008) 1333-1345.

[5] H. Sovovà, R.P. Stateva, Supercritical fluid extraction from vegetable materials, Reviews in Chemical Engineering, 27 (2011) 79-156.

[6] J.M. del Valle, J.C. de la Fuente, Supercritical CO2 extraction of oilseeds: Review of kinetic and equilibrium models, Critical Reviews in Food Science and Nutrition, 46 (2006) 131-160.

[7] Z. Huang, X.H. Shi, W.J. Jiang, Theoretical models for supercritical fluid extraction, Journal of Chromatography A, 1250 (2012) 2-26.

[8] E.L.G. Oliveira, A.J.D. Silvestre, C.M. Silva, Review of kinetic models for supercritical fluid extraction, Chemical Engineering Research and Design, 89 (2011) 1104-1117.

[9] T. Funazukuri, C.Y. Kong, S. Kagei, Binary diffusion coefficients in supercritical fluids: Recent progress in measurements and correlations for binary diffusion coefficients, Journal of Supercritical Fluids, 38 (2006) 201-210.

[10] I. Medina, Determination of diffusion coefficients for supercritical fluids, Journal of Chromatography A, 1250 (2012) 124-140.

[11] M. Škerget, Z. Knez, M. Knez-Hrnčič, Solubility of solids in sub- and supercritical fluids: A review, Journal of Chemical and Engineering Data, 56 (2011) 694-719.

[12] K.Y. Foo, B.H. Hameed, Insights into the modeling of adsorption isotherm systems, Chemical Engineering Journal, 156 (2010) 2-10.

[13] A. Salimi, S. Fatemi, H.Z. Nei Nei, A. Safaralie, Mathematical modeling of supercritical extraction of valerenic acid from Valeriana officinalis L, Chemical Engineering and Technology, 31 (2008) 1470-1480.

[14] J.M. del Valle, F.A. Urrego, Free solute content and solute-matrix interactions affect apparent solubility and apparent solute content in supercritical CO 2 extractions. A hypothesis paper, Journal of Supercritical Fluids, 66 (2012) 157-175.

[15] M. Goto, B.C. Roy, A. Kodama, T. Hirose, Modeling supercritical fluid extraction process involving solute-solid interaction, Journal of Chemical Engineering of Japan, 31 (1998) 171-177.

[16] M. Perrut, J.Y. Clavier, M. Poletto, E. Reverchon, Mathematical Modeling of Sunflower Seed Extraction by Supercritical CO2, Industrial and Engineering Chemistry Research, 36 (1997) 430-435.
[17] E. Reverchon, Mathematical Modeling of Supercritical Extraction of Sage Oil, AIChE Journal, 42 (1996) 1765-1771.
[18] F.A. Urrego, G.A. Núñez, Y.D. Donaire, J.M. del Valle, Equilibrium partition of rapeseed oil between supercritical CO2 and prepressed rapeseed, Journal of Supercritical Fluids, 102 (2015) 80-91.
[19] D. Djohan, Q. Yu, D.W. Connell, Partition isotherms of chlorobenzenes in a sediment-water system, Water, Air, and Soil Pollution, 161 (2005) 157-173.
[20] K.M. Hangos, I.T. Cameron, Process modelling and model analysis, Academic Press, San Diego, CA, 2001.
[21] L.P.S. Silva, J. Martínez, Mathematical modeling of mass transfer in supercritical fluid extraction of oleoresin from red pepper, Journal of Food Engineering, 133 (2014) 30-39.
[22] A. Osberghaus, S. Hepbildikler, S. Nath, M. Haindl, E. von Lieres, J. Hubbuch, Determination of parameters for the steric mass action model-A comparison between two approaches, Journal of Chromatography A, 1233 (2012) 54-65.
[23] A. Rai, K.D. Punase, B. Mohanty, R. Bhargava, Evaluation of models for supercritical fluid extraction, International Journal of Heat and Mass Transfer, 72 (2014) 274-287.
[24] M. Stamenic, J. Ivanovic, S. Grujic, S. Milovanovic, I. Zizovic, S. Petrovic, Comparative analysis of mathematical models for supercritical extraction simulation from industrially valuable lamiaceae herbs, Canadian Journal of Chemical Engineering, 92 (2014) 75-81.
[25] O. Döker, U. Salgin, I. Şanal, Ü. Mehmetoğlu, A. Çalimli, Modeling of extraction of β-carotene from apricot bagasse using supercritical CO2 in packed bed extractor, Journal of Supercritical Fluids, 28 (2004) 11-19.
[26] H. Sovová, Rate of the vegetable oil extraction with supercritical CO2-I. Modelling of extraction curves, Chemical Engineering Science, 49 (1994) 409-414.
[27] H. Sovová, Mathematical model for supercritical fluid extraction of natural products and extraction curve evaluation, Journal of Supercritical Fluids, 33 (2005) 35-52.
[28] V. Abrahamsson, I. Rodriguez-Meizoso, C. Turner, Supercritical fluid extraction of lipids from linseed with on-line evaporative light scattering detection, Anal Chim Acta, 853 (2015) 320-327.
[29] G. Andrich, S. Balzini, A. Zinnai, V. De Vitis, S. Silvestri, F. Venturi, R. Fiorentini, Supercritical fluid extraction in sunflower seed technology, European Journal of Lipid Science and Technology, 103 (2001) 151-157.
[30] G. Andrich, A. Zinnai, U. Nesti, F. Venturi, R. Fiorentini, Supercritical fluid extraction of oil from microalga Spirulina (Arthrospira) platensis, Acta Alimentaria, 35 (2006) 195-203.
[31] K.D. Bartle, A.A. Clifford, S.B. Hawthorne, J.J. Langenfeld, D.J. Miller, R. Robinson, A model for dynamic extraction using a supercritical fluid, The Journal of Supercritical Fluids, 3 (1990) 143-149.
[32] T. Veress, Sample preparation by supercritical fluid extraction for quantification a model based on the diffusion-layer theory for determination of extraction time, Journal of Chromatography A, 668 (1994) 285-291.
[33] IUPAC. Compendium of Chemical Terminology, 2nd ed. (the "Gold Book"). Compiled by A. D. McNaught and A. Wilkinson. Blackwell Scientific Publications, Oxford (1997). XML on-line corrected version:

http://goldbook.iupac.org (2006-) created by M. Nic, J. Jirat, B. Kosata; updates compiled by A. Jenkins. ISBN 0-9678550-9-8. doi:10.1351/goldbook.

[34] B. Seifried, F. Temelli, Viscosity and rheological behaviour of carbon dioxide-expanded fish oil triglycerides: Measurement and modeling, Journal of Supercritical Fluids, 59 (2011) 27-35.

[35] G. Guiochon, D.G. Shirazi, A. Felinger, A.M. Katti, Fundamentals of Preparative and Nonlinear Chromatography, Academic Press, 2006.

[36] N. Borg, Y. Brodsky, J. Moscariello, S. Vunnum, G. Vedantham, K. Westerberg, B. Nilsson, Modeling and robust pooling design of a preparative cation-exchange chromatography step for purification of monoclonal antibody monomer from aggregates, Journal of Chromatography A, 1359 (2014) 170-181.

[37] E.W. Lemmon, M.O. McLinden, D.G. Friend, Thermophysical Properties of Fluid Systems, in: P.J. Linstrom, W.G. Mallard (Eds.) NIST Chemistry WebBook, NIST Standard Reference Database Number 69, http://webbook.nist.gov/chemistry/fluid, (retreived August 1, 2014).

[38] M.B. King, T.R. Bott, M.J. Barr, R.S. Mahmud, Equilibrium and rate data for the extraction of lipids using compressed carbon dioxide, Separation Science and Technology, 22 (1985) 1103-1120.

[39] J. Puiggené, M.A. Larrayoz, F. Recasens, Free liquid-to-supercritical fluid mass transfer in packed beds, Chemical Engineering Science, 52 (1997) 195-212.

[40] C.-S. Tan, S.-K. Liang, D.-C. Liou, Fluid-solid mass transfer in a supercritical fluid extractor, Chemical engineering journal, 38 (1988) 17-22.

[41] N. Wakao, T. Funazkri, Effect of fluid dispersion coefficients on particle-to-fluid mass transfer coefficients in packed beds. Correlation of sherwood numbers, Chemical Engineering Science, 33 (1978) 1375-1384.

[42] R.V. Vaz, A.L. Magalhães, C.M. Silva, Improved Stokes–Einstein based models for diffusivities in supercritical CO2, Journal of the Taiwan Institute of Chemical Engineers, 45 (2014) 1280-1284.

[43] D. Fennell Evans, T. Tominaga, C. Chan, Diffusion of symmetrical and spherical solutes in protic, aprotic, and hydrocarbon solvents, Journal of Solution Chemistry, 8 (1979) 461-478.

[44] A.L. Magalhães, P.F. Lito, F.A. Da Silva, C.M. Silva, Simple and accurate correlations for diffusion coefficients of solutes in liquids and supercritical fluids over wide ranges of temperature and density, Journal of Supercritical Fluids, 76 (2013) 94-114.

[45] P. Chang, C.R. Wilke, Some measurements of diffusion in liquids, The Journal of Physical Chemistry, 59 (1955) 592-596.

[46] E. Reverchon, G. Donsì, L.S. Osséo, Modeling of supercritical fluid extraction from herbaceous matrices, Industrial and Engineering Chemistry Research, 32 (1993) 2721-2726.

[47] J.M. del Valle, J.C. de la Fuente, E. Uquiche, A refined equation for predicting the solubility of vegetable oils in high-pressure CO 2, Journal of Supercritical Fluids, 67 (2012) 60-70.

[48] J.M. del Valle, J.M. Aguilera, An improved equation for predicting the solubility of vegetable oils in supercritical CO2, Industrial and Engineering Chemistry Research, 27 (1988) 1551-1553.

[49] H. Sovová, M. Zarevúcka, M. Vacek, K. Stránský, Solubility of two vegetable oils in supercritical CO2, Journal of Supercritical Fluids, 20 (2001) 15-28.

[50] J. Chrastil, Solubility of solids and liquids in supercritical gases, Journal of Physical Chemistry, 86 (1982) 3016-3021.
[51] R.J. LeVeque, Finite Volume Methods for Hyperbolic Problems, in, Cambridge University Press, Cambridge, 2002.
[52] A.I. El-Gallad, M.E. El-Hawary, A.A. Sallam, Swarming of intelligent particles for solving the nonlinear constrained optimization problem, International Journal of Engineering Intelligent Systems for Electrical Engineering and Communications, 9 (2001) 155-163.
[53] D.C. Montgomery, Design and Analysis of Experiments, 7th ed., Wiley, Hoboken, NJ, 2009.
[54] M. Stamenic, I. Zizovic, R. Eggers, P. Jaeger, H. Heinrich, E. Rój, J. Ivanovic, D. Skala, Swelling of plant material in supercritical carbon dioxide, Journal of Supercritical Fluids, 52 (2010) 125-133.
[55] S. Chatterjee, C. Carrera, L.A. Lynch, Genetic algorithms and traveling salesman problems, European Journal of Operational Research, 93 (1996) 490-510.